Ocular Pharmacokinetic Study Using T₁ Mapping and Gd-Chelate-Labeled Polymers

Xianfeng Shi • Xin Liu • Xueming Wu • Zheng-Rong Lu • S. Kevin Li • Eun-Kee Jeong

ABSTRACT

Purpose Recent advances in drug discovery have led to the development of a number of therapeutic macromolecules for treatment of posterior eye diseases. We aimed to investigate the clearance of macromolecular contrast probes (polymers conjugated with Gd-chelate) in the vitreous after intravitreal injections with the recently developed ms-DSEPI-T12 MRI and to examine the degradation of disulfide-containing biodegradable polymers in the vitreous humor *in vivo*.

Methods Intravitreal injections of model contrast agents poly[N-(2-hydroxypropyl)methacrylamide]-GG-1,6-hexanediamine-(Gd-DO3A), biodegradable (Gd-DTPA)-cystine copolymers, and MultiHance were performed in rabbits; their distribution and elimination from the vitreous after injections were determined by MRI.

Results Times for macromolecular contrast agents to decrease to half their initial concentrations in the vitreous ranged from 0.4–1.3 days post-injection. Non-biodegradable polymers demonstrated slower vitreal clearance than those of disulfide-biodegradable polymers. Biodegradable polymers had similar clearance as MultiHance.

Conclusions Usefulness of T₁ mapping and ms-DSEPI-T12 MRI to study ocular pharmacokinetics was demonstrated. Results suggest an enzymatic degradation mechanism for the disulfide linkage in polymers in the vitreous leading to breakup of polymers in vitreous humor over time.

KEY WORDS biodegradable polymer · MRI · ms-DSEPI-T12 · ocular pharmacokinetics · vitreous humors

INTRODUCTION

In recent years, significant advances have been made in the treatment of blindness-related eye diseases such as age-related macular degeneration and diabetic retinopathies. For diseases of the anterior parts of the eye, the common route of administration is topical eye drop. However, topical administration generally does not effectively deliver drugs to the tissues at the back of the eye. Systemic administration is usually not preferred because of the resulting systemic toxicity. An effective and robust drug delivery system for the treatment of posterior segment diseases is still not available. Intravitreal injection remains the preferred route of drug administration to the posterior segment of the eye (1–3).

Biodegradable polymers have been employed in targeted drug delivery in the eye and as a drug delivery matrix for sustained ocular delivery (4,5). Disulfide-containing polymers have been used as biomaterial platforms in the development of drug and gene delivery systems due to their biocompatibility and targetability (6). For example, these reduction-sensitive drug delivery systems have been evaluated as bioresponsive polymeric nanocarriers and temperature sensitivity block copolymers (4,7). One of the characteristics of the disulfide linkages is that at times the

X. Shi · X. Liu · E.-K. Jeong (✉)
Department of Radiology
Utah Center for Advanced Imaging Research, University of Utah
729 Arapeen Dr.
Salt Lake City, Utah 84108, USA
e-mail: ekj@ucair.med.utah.edu

X. Wu · Z.-R. Lu
Department of Biomedical Engineering
Case Western Reserve University
Cleveland, Ohio, USA

S. K. Li
Division of Pharmaceutical Sciences, College of Pharmacy
University of Cincinnati
Cincinnati, Ohio, USA

disulfide bond can be relatively stable in body fluids but can go through rapid cleavage under other conditions such as enzymatic degradation. The study of ocular distribution of disulfide-biodegradable synthetic polymers in the eye could help pharmaceutical scientists understand the drug delivery mechanism and clearance after intravitreal administration of these drug delivery systems.

Improvement of eye disease treatment based on novel drug delivery methods depends on reliable pharmacokinetics data and the understanding of drug delivery and clearance mechanisms in the eye (8,9). The investigation of ocular pharmacokinetics by traditional methods is invasive and can severely disturb the biodistribution of pharmaceuticals during dissection in animals (10). Recent studies have demonstrated the feasibility of MRI for noninvasive monitoring of the biodistribution of pharmaceuticals in the body in drug delivery research (9,11–13). MRI is particularly useful in ocular research to study, for example, the flux-enhancing mechanisms of ocular iontophoresis, the release kinetics from an ocular implant, the least resistive route for transscleral penetration, and the locations of the periocular and intraocular depots in periocular, intrascleral, and intravitreal administration (10,14–22). In these MRI studies, quantitative measurements of the concentration of contrast agent were performed by comparing the signal intensities of the voxel in the region of interest (ROI) and a calibration curve. The calibration curves were constructed by MRI of contrast agent solution standards or standards of contrast agent in hydroxypropyl methylcellulose. This method of converting the signal intensity to contrast agent concentration can be affected by errors such as variability due to MRI hardware, coil positioning, and experimental setup as well as by the non-linear signal intensity-to-concentration relationship.

In the present study, a new quantitative method was employed in an MRI study of macromolecules conjugated with gadolinium-chelate (Gd-chelate) that were injected into the vitreous of the rabbit eye. These macromolecules are drug surrogates to study the clearance of macromolecules in ocular drug delivery. For the accurate quantification of the contrast agent concentration, the change in the relaxation rate ($\Delta R1$) was measured using 3D multishot double spin echo-planar imaging with automated variation of TR and TE (ms-DSEPI-T12) (23), which offers rapid and dynamic T_1 measurement; ΔR_1 is known to be directly proportional to the concentration of the Gd-based contrast agent, unlike MRI signal intensity, which is not linear to the local concentration of the paramagnetic ion. The objectives of the present study were therefore to (a) demonstrate the applicability of the ms-DSEPI-T12 method in MRI ocular pharmacokinetic study, (b) examine disulfide bond degradation in the vitreous humor with polymerized biodegradable/non-

biodegradable compounds, and (c) study the clearance of macromolecules in the vitreous after intravitreal injections with MRI.

MATERIALS AND METHODS

Materials

Polymers poly[N-(2-hydroxypropyl)methacrylamide]-GlyGly-1,6-hexanediamine-(Gd-DO3A) (abbreviation: PHPMA-GG-1,6-hexanediamine-(Gd-DO3A) or PGH) of molecular weights 20 kDa and 90 kDa were synthesized using a method similar to that described previously (24). The polymers were then prepared in saline at concentration of 1.3 µmol-Gd per mL. Biodegradable polymers (Gd-DTPA)-cystine copolymers (abbreviation: GDCP) of molecular weights 21 kDa and 144 kDa were synthesized as described previously (25) and prepared in saline at concentration of 1.3 µmol-Gd per mL. The molecular structures of PGH and GDCP are shown in Fig. 1a, b, respectively. MultiHance™ (Bracco Diagnostics, Inc.) was prepared in saline at the same concentration (1.3 µmol-Gd per mL) and used as a reference.

MRI Phantom Experiment

MRI studies were performed on a Clinical 3T MRI system (Trio, Siemens Medical Solutions, Erlangen, Germany) with Avanto gradients (45 mT/m strength and 200 T/m/s slew rate) at room temperature (~25°C). Phantom experiments were conducted to determine the relationship between signal intensity and six GDCP (144 kDa) concentrations. T_1 relaxivity was measured using inversion-recovery spin-echo on a series of phantoms filled with different concentrations of PGH_{20}, PGH_{90}, $GDCP_{21}$, and MultiHance™. 12-element receive-only coil with body coil excitation was used on phantom with the following scan parameters: FOV=200× 150 mm², matrix size=256×192, slice thickness=2.5 mm, TR/TE=5000/16 ms, inversion recovery time=25, 35, 50, 75, 100, 200, 400, 800 and 1600 ms, respectively.

MRI Animal Experiment

New Zealand White rabbits (weight ~3 kg) were used with the approval of the Institutional Animal Care and Usage Committee at the University of Utah. The animals were anesthetized by the intramuscular injection of a cocktail of 1 ml Ketamine (100 mg/ml) and 1 ml Xylazine (15 mg/ml). Intravitreal injections of 100 µL PGH or GDCP at 1.3 µmol-Gd per mL were performed using a 0.5-inch 29-gauge needle at the pars plana. Intravitreal injections of a corresponding dose of Multihance™ were performed on the opposite eyes
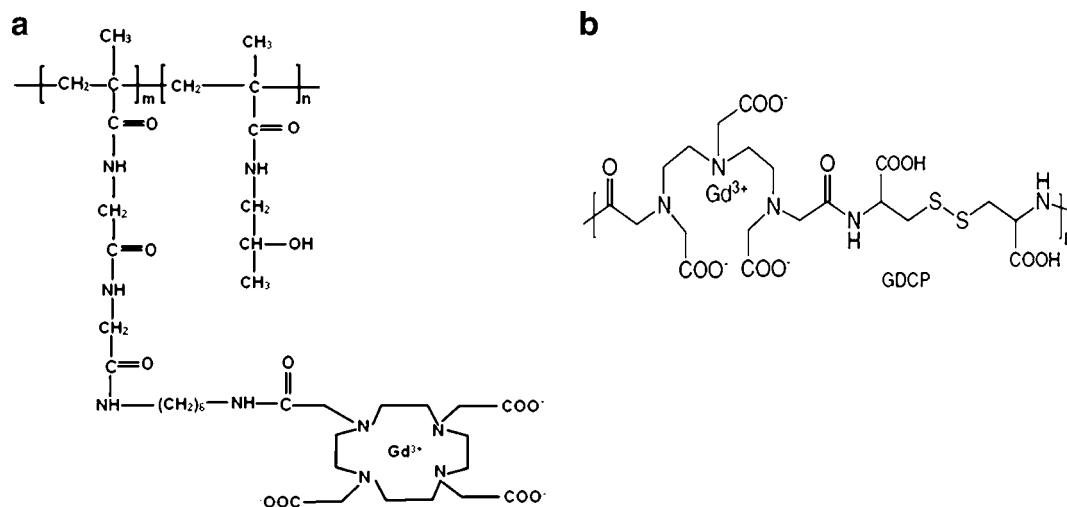
Fig. 1 (**a**) PHPMA-GG-1,6-hexanediamine-(Gd-DO3A). (**b**) GDCP: (Gd-DTPA)-Cystine copolymers.

using the same procedure. Following the injections, rabbit MRI was performed on the Clinical 3T MRI system. After the MRI scans, the animals were returned to their cage and allowed normal access to food and water.

T_1 weighted spin echo and saturation-recovery multishot spin-echo EPI (3D multishot double spin-echo EPI: 3D ms-DSEPI-T12) pulse sequences were applied at each dynamic time point to acquire the T_1 weighted-spin echo images and T_1 maps, respectively. The *in vivo* T_1 relaxation times were measured before and after contrast agent injection into the vitreous humor. Briefly, in T_1 and T_2 mapping imaging using 3D ms-DSEPI-T12 (23), the recovery times (TR) and the echo times (TE) that are relevant time variables for the fitting were varied automatically within the pulse sequence for entire data collection. The imaging parameters for the T_1 weighted imaging were $0.4 \times 0.4 \times 1.0$ mm^3 spatial resolution, 256×160 acquisition matrix, receiver bandwidth 250 Hz/pixel, and TR/TE 602/11 ms. Images were acquired consecutively before and at different time points after the injection of PGH, GDCP, and MultiHance™. The imaging parameters for the T_1 mapping were FOV $128 \times 40 \times 24$ mm^3, acquisition matrix $128 \times 40 \times 12$, spatial resolution $1.0 \times 1.0 \times 2.0$ mm^3, receiver bandwidth of 1.086 kHz/pixel, echotrain length (ETL) 7, and TRs/TEs of 138/32, 338/42, 738/52, 1528/62, 2318/72 and 3108/82 ms. The total scan time for each time-point was 6 min.

Data Processing

Rabbit vitreous humor T_1 maps were calculated for each slice using a non-linear least-squares three-parameter fitting algorithm for a given time point. The *in vivo* T_1 relaxation time is then used to construct the change in the relaxation rate using $\Delta R_1 = \left(\frac{1}{T_1(C)} - \frac{1}{T_1(0)} \right)$. The temporal change of T_1 relaxation rates in rabbit vitreous following a contrast

agent injection was investigated by summing ΔR_1 over the whole vitreous humor. For a given animal, rabbit eye anatomical region was manually segmented to cover the whole vitreous humor. Because the concentration of the contrast agent is proportional to the T_1 relaxation rates, $\Delta R_1 = r_1 C_{molecule}$, where r_1 is the molecule relaxivity and $C_{molecule}$ is the concentration of the contrast agent, the amount of the contrast agent in each voxel is proportional to T_1. The total average concentration of the contrast agent in the vitreous (C_{total}) at each time point (or the total amount of contrast agent in the vitreous humor divided by the volume of the vitreous) can therefore be calculated:

$$C_{total} = \frac{\sum (C_{molecule} \cdot V_{voxel})}{V_{voxel} \mathcal{N}_{voxel}} - \text{background}$$

$$= \frac{\sum (\Delta R_1 / r_1)}{\mathcal{N}_{voxel}} - \text{background} \qquad (1)$$

where $\mathcal{N}_{voxel}$ is the total number of voxel in the measurement, V_{voxel} is the voxel volume, and background is the value determined using the same method but with control rabbits without the injection of the contrast agent. The relaxivity r_1 was measured using phantoms containing the contrast agent (see T_1 relaxivity presented in Table I). The concentration-time profiles of the contrast agent in the vitreous were then analyzed.

Table I T_1 Relaxivity of GDCP, MultiHance and PGH

	GDCP		MultiHance™	PGH	
Molecular Weight (kDa)	21	144	1.1	20	90
T_1 relaxivity (r_1) (mM^{-1}s^{-1})	5.4	8.2	4.2	11.7	10.9

RESULTS

MRI Phantom Experiment: T$_1$ Relaxivity of GDCP, MultiHance, and PGH

Figure 2a, b presents the representative profiles of the changes of the relative signal intensity and the relaxation rate ΔR_1 as a function of GDCP concentration. The relative signal intensity was defined as the ratio of images acquired with GDCP and reference image without GDCP, which were measured using the inversion recovery spin echo pulse sequence. The relationship between the signal intensity and the Gd concentration is non-linear, as illustrated in Fig. 2a, where the negative sign of signal intensity indicates the inverted longitudinal magnetization vector (anti-parallel to the applied magnetic field B$_0$) after 180° inversion RF pulse. The non-linear relationship between signal intensity (SI) and contrast agent concentration could introduce substantial errors in estimating the concentration and the subsequent pharmacokinetic evaluation. On the contrary, the change of inverse T$_1$ exhibits linear correlation with respect to GDCP concentration as shown in Fig. 2b.

Table I summarizes the T$_1$ relaxivities of the contrast agents in the present study. T$_1$ relaxivity for gadolinium-based chelates is determined mainly by three factors: the exchange time between the water molecule being bound to the Gd and in bulk solution, the electron relaxation time of Gd, and the tumbling time of Gd. As the molecular weight increases, the longer tumbling time allows the other two factors to dominate. Relaxivity among biodegradable polymers GDCP$_{144}$ and GDCP$_{21}$ increases with increasing polymer molecular weight. For the non-biodegradable polymers PGH$_{20}$ and PGH$_{90}$, the polymer molecular weight does not significantly affect PGH relaxivity.

### MRI Animal Experiment: Ocular Clearance After Intravitreal Injection

Figure 3a, b shows the representative MR images at different stages after the injection of non-biodegradable PGH$_{20}$ (left) and MultiHance (right) and biodegradable GDCP$_{21}$ (left) and MultiHance (right), respectively. The MR images show clear differences between the post-injection distributions of PGH$_{20}$, GDCP$_{21}$, and MultiHance in the rabbit eyes. MultiHance was administered into the vitreous for comparison. Due to the introduction of these contrast agents, T$_1$ value near the administration site was shortened, and signal intensity around the administration site was enhanced: these sites are demonstrated by white arrows in Fig. 3a, b. The MR images of MultiHance and GDCP$_{21}$ show that signal enhancement disappears around 1 day after intravitreal administration. Figure 4a shows the representative T$_1$ maps of non-biodegradable PGH$_{20}$ (left) and MultiHance (right). Unlike signal intensity contrast images that usually have coupling effects of multiple mechanisms, T$_1$ map contrast is uniquely determined by relative T$_1$ amplitude in the vitreous region, which is dynamically altered as contrast agent diffuses and clears out. In the present experiment, a significant amount of PGH was observed even after 3 days based on the T$_1$ maps. On the contrary, MultiHance shows rapid clearance from the vitreous compared to PGH. Figure 4b presents the T$_1$ maps of GDCP and MultiHance in similar experimental settings. The arrows point to the administration sites. The data show that clearance of GDCP from the vitreous is faster than that of PGH.

The concentration-time profiles of PGH in the vitreous are plotted in Fig. 5a. During the early time period post-injection, PGH$_{90}$ concentration increases with time after the injection and then gradually decreases over time from approximate 4 h after injection to the end of the
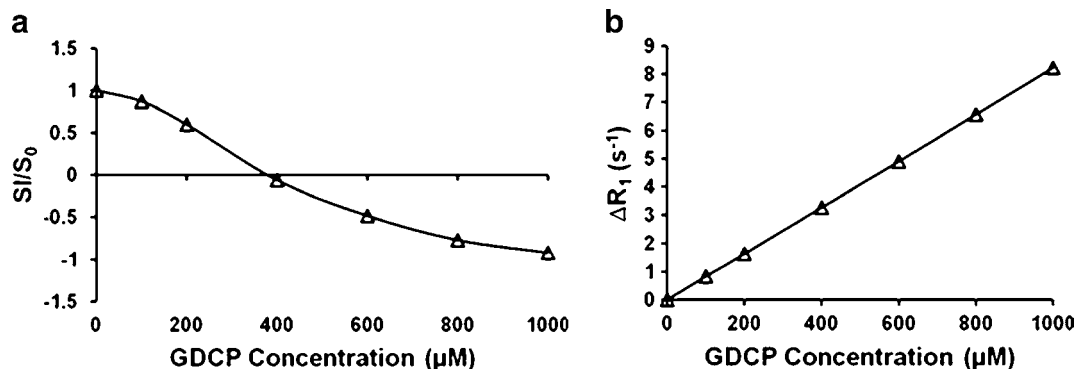

Fig. 2 Plots of (**a**) inversion-recovery spin-echo signal intensity and (**b**) ΔR_1 with respect to GDCP concentration in solution phantom. SI and S$_0$ are signal intensity acquired with and without GDCP in phantom, respectively. Negative sign in signal intensity indicates inverted longitudinal magnetization vector after 180° inversion RF pulse.

Fig. 3 Representative T_1 weighted spin echo images for (**a**) PGH₂₀ (L) and MultiHance (R) and (**b**) GDCP₂₁ (L) and MultiHance (R), where L and R represent left eye and right eye, respectively. Day, hour and minute are abbreviated as d, h and min, respectively. White arrows show the injection sites of the contrast agents.
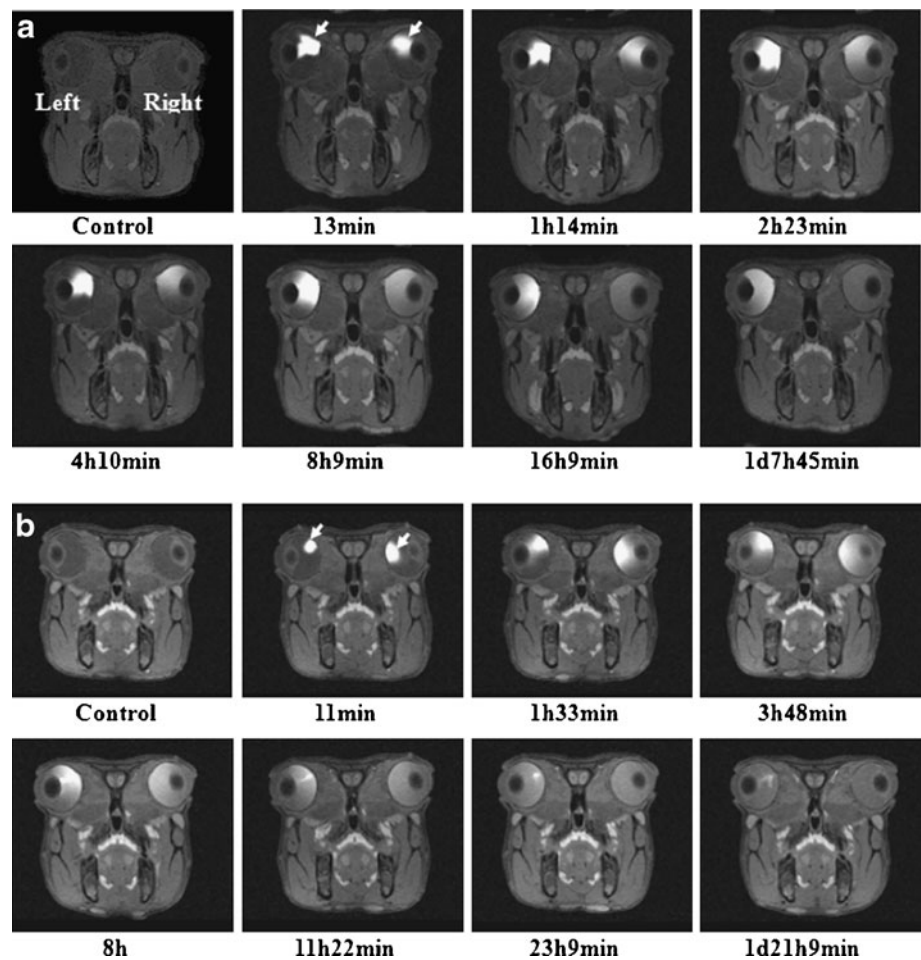
Fig. 4 Representative time varied T_1 map computed using MR images acquired with ms-DSEPI-TI2 for (**a**) PGH₂₀ (L) and MultiHance (R) and (**b**) GDCP₂₁ (L) and MultiHance (R), respectively. White arrows show the injection sites of the contrast agents.
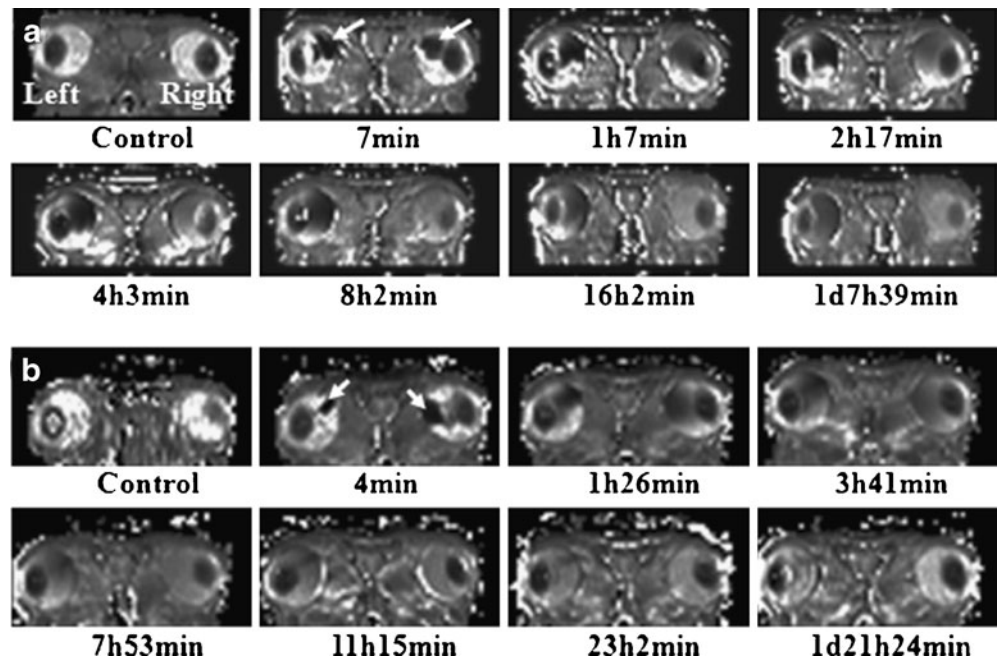
Fig. 5 Concentration-time profile of (**a**) non-biodegradable PGH (20 and 90 kDa) and (**b**) biodegradable GDCP (21 and 144 kDa). The concentration-time profiles of MultiHance in (**a**) and (**b**) are shown as reference.
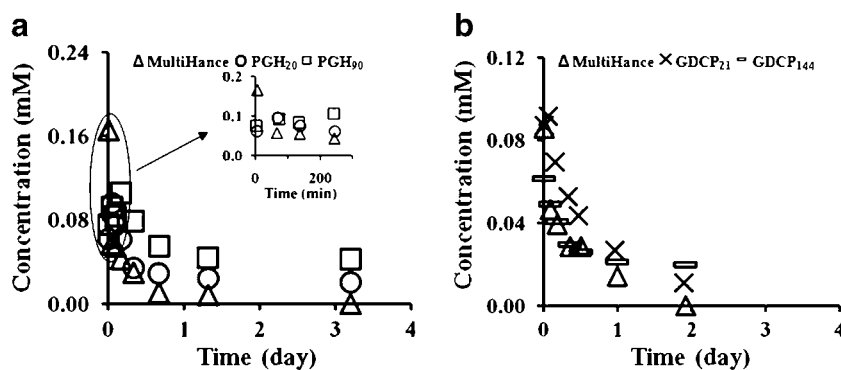
experiment. The increase of the mean concentration in the vitreous at the first several time points after injection is puzzling and likely related to T_1 overestimation that will be discussed later in the Discussion section. From the results in Fig. 5a, a significant amount of PGH_{90} was still observed in the vitreous even at 3 days post-injection. A similar trend in the PGH_{20} concentration profile was observed. PGH_{20} concentration reaches its maximum around 2 h after the injection and is cleared faster from the vitreous than PGH_{90}. These plots suggest that clearance for the non-biodegradable polymers is a slow process in the vitreous and is related to the molecular weight of the polymers.

In Fig. 5a, different clearance behavior was observed in concentration-time plot of MultiHance compared with that of PGH. MultiHance does not show an initial increase in concentration, and its concentration decreases quickly with time until all residual MultiHance is cleared. For GDCP in Fig. 5b, the biodegradable polymers exhibit different clearance patterns compared to those of PGH. Both $GDCP_{21}$ and $GDCP_{144}$ concentrations in the vitreous humor decrease relatively quickly over time. For example, the biodegradable polymers show a similar decrease in concentration as that of MultiHance in the first day, different from that of PGH_{90}. Comparing the concentration of GDCP, PGH, and MultiHance, the times of $GDCP_{21}$, $GDCP_{144}$, and MultiHance to decrease to half of their initial concentrations (i.e., their initial half-lives) in the vitreous after intravitreal injection are approximately 0.5, 0.4, and 0.15 days, and those of PGH_{20} and PGH_{90} are 0.5 and 1.3 days, respectively. The clearance of a molecule in the vitreous humor is expected to follow a monoexponential decay function when the molecule diffuses in the vitreous and eliminated at the retina or the anterior chamber. However, the concentration-time profiles in the vitreous for the studied polymers, particularly PGH_{20} and PGH_{90}, did not fit well with a first-order mono-exponential decay function. This can also be illustrated by following the concentration-time decrease profiles from 50% to 25% of their initial values in the figure. The times

of PGH_{20} and PGH_{90} to decrease to 25% of their initial concentration in the vitreous are approximately 1.4 and 6 days post-injection, about 3 and 5 times of their respective initial half-lives.

DISCUSSION

MRI Ocular Pharmacokinetic Studies

Ocular drug delivery has been a recent interest among ophthalmologists and pharmaceutical researchers, partly due to the lack of an effective drug delivery system for the treatment of posterior eye diseases. Previous MRI pharmacokinetic studies of the eye have demonstrated the advantages of the noninvasive MRI approach. However, quantitative measurements of the concentration of contrast agent in these MRI studies relied on a signal intensity *versus* contrast agent concentration calibration curve constructed by MRI of contrast agent standards, which can be compromised by errors such as variability of coil positioning and experimental setup. In addition, the relationship between image signal intensity and contrast agent concentration was not linear, as the image signal intensity is intrinsically determined not only by T_1 relaxation but also T_2 relaxation mechanisms. Most methods for T_1 measurement are time-consuming and unsuitable for dynamic pharmacokinetic study. In the present study, a recently developed MR technique (ms-DSEPI-T12) was used to dynamically map the T_1 of the contrast agents in the vitreous humor; the scan time was 6 min in the present MRI setting. This powerful technique has the potential to measure rapid T_1 changes due to the clearance of contrast agents from the vitreous as demonstrated in the present study.

The study of disulfide bond biodegradable polymers in the vitreous humor can provide information on the clearance mechanism and degradation kinetics of disulfide linkage in the vitreous in the development of novel drug delivery systems to deliver therapeutics to the posterior eye. The present study examined the degradation of disulfide

bonds in the vitreous humor. The comparison of the clearance of biodegradable polymers GDCP, non-biodegradable polymers PGH, and MultiHance suggests that GDCP were broken into smaller fragments in the vitreous humor within a day after intravitreal administration. It was originally thought that disulfide-containing biodegradable polymers have slow polymer degradation in the vitreous and thus can be utilized as matrices in ocular drug delivery systems such as bioresponsive polymeric nanocarrier and temperature sensitivity copolymer drug delivery systems for sustained drug delivery in the eye. In general, slow-degrading polymers are required to provide effective sustained ocular delivery for the treatment of chronic eye diseases, and, ideally, drug administration through the intravitreal route such as injection or implant is preferred to have longer than 1-month interval. The relatively fast and noticeable disulfide degradation in the vitreous humor shown in the present study suggests that this type of polymer may not be suitable for long sustained drug delivery (e.g., over 1 month) in chronic posterior eye disease therapy.

Experimental Errors, Assumptions, and Their Effects

The concentration of the contrast agents in the present study was determined by T_1 relaxivities of the contrast agents. Unlike contrast agents in tissues that *in vivo* T_1 relaxivities are likely different from the *in vitro* values, the vitreous humor generally can be assumed as uniform in character and the observed relaxivity values of the polymers in solutions *in vitro* can be assumed approximately equivalent to those in the vitreous *in vivo*. This assumption is appropriate in the PGH and Multihance analyses. For GDCP, a caveat is that the observed relaxivities for the biodegradable GDCP could consistently be changing when the molecular weight decreases over time due to polymer degradation in the vitreous.

Temperature difference between MRI experiments *in vivo* (26) and those of phantoms at room temperature *in vitro* could be another source of errors due to the possible effect of temperature on T_1 relaxivity. According to theory, the change in relaxation rate $(1/T_1)$ contributed through the paramagnetic ion (Gd) is directly related to the change in the molecular motion of the contrast agent. For a contrast agent with relatively high molecular weight (e.g., 20–144 kDa), it is not likely that the molecular motion varies significantly between room and body temperature. The effect of temperature on relaxivity of Gd-chelate polymers has been described in a previous study (27) in which less than 5% change of relaxivity was observed within the temperature range from 26 to 37°C. The difference in the temperatures in the present *in vivo* and *in vitro* MRI experiments therefore is not expected to significantly impact the conclusions of the present study.

Another experimental error was related to the increase in the mean total concentration of the contrast agent in vitreous humor in the first several time points after the injection of PGH as illustrated in Fig. 5a. Once the Gd-chelated compound was injected into the vitreous, a decline in the total vitreous concentration over the duration of the experiment was expected. This abnormal behavior probably resulted from T_1 overestimation. In the T_1 relaxivity calculation, the saturation recovery signal intensity curve was used to determine the T_1 value. The available minimum saturation recovery time is limited to 138 ms in the present imaging technique. If the T_1 value near the administration site of PGH is shorter than 100 ms, curve-fitting routine may introduce an error in the resultant T_1 value under the effect of noise. The fitting on these signal curves would result in the overestimation of T_1 value. As the concentration in local region decreases, overestimation of T_1 diminishes when the longer true T_1 relaxation time is greater than 138 ms.

Ocular Clearance of Macromolecules

Previous studies have shown that the half-lives of vitreal clearance of ranibizumab (Lucentis) and bevacizumab (Avastin), which have molecular weight of 48 k and 149 k Dalton, are 2.9 and 4.3 days, respectively, in rabbits (28,29). For rituximab, another antibody, the half-life of the macromolecule in vitreous was 4.7 days (30). FITC-dextran of 66 k Dalton in the vitreous after intravitreal administration has a clearance rate of 0.005 h^{-1}, this corresponding to apparent half-life of ~5 days (31,32). The clearance of MRI contrast agent Gd-labeled albumin (Galbumin) in the vitreous was studied and found to have apparent initial half-life of 2 days after 1 mg/mL intravitreal injection (22). In the present intravitreal study, the times of PGH_{90} to decrease to half and one-fourth of its initial concentration were 1.3 and 6 days, respectively, within the same order of magnitude compared to these macromolecules in the literature.

Based on Einstein diffusion theory, the molecular translational diffusivity is inversely proportional to $\sqrt{m}$ as $D \propto 1/\sqrt{m}$, and the mean displacement is $l = \sqrt{6D\tau}$, where m and τ represent the molecular mass and diffusion time, respectively. Molecules with higher molecular weight diffuse at slower rates, take longer time to spread in the vitreous, and have slower clearance rates. As illustrated in the present study, PGH_{20} has a faster clearance rate than PGH_{90}. Similarly, MultiHance shows faster clearance compared with PGH_{20} and PGH_{90}. These results are consistent with the diffusion theory. On the other hand, $GDCP_{21}$ and $GDCP_{144}$ have similar clearance *vs.* time patterns, possibly due to their degradable nature. $GDCP_{144}$ or $GDCP_{21}$ can degrade into smaller molecules during the

course of diffusion in the vitreous, and the smaller GDCP fragments have faster clearance from the vitreous. These GDCP results suggest fast degradation of disulfide-containing polymers (disulfide bond) in the vitreous, possibly due to the presence of disulfide bond enzymes in the vitreous humor.

Although the clearance of macromolecules is hypothesized to be predominantly through the anterior route (32,33), there is no significant increase in the signal in the anterior chamber in the experiments with PGH. This may be due to the fast clearance in the anterior chamber (volume ~0.3 mL with aqueous humor turnover rate ~0.1 mL/hr (34)) resulting in PGH concentration below the MRI detection limit in the anterior chamber. PGH can also be cleared at the uvea/ciliary body as the main elimination pathway before PGH enters the anterior chamber. It is also possible that posterior clearance remained the main ocular elimination route for the macromolecule. Further investigation on the clearance mechanism of macromolecules after intravitreal administration, such as using Gd-labeled polymers at higher concentrations, is required to study the clearance route of macromolecules. For GDCP, due to the degradation of the polymers and the similar clearance rate between GDCP and MultiHance as illustrated in Fig. 5b, it is likely that these biodegradable polymers are cleared through the retina.

CONCLUSION

The distribution and clearance of PGH and GDCP in the vitreous after intravitreal injections were studied in rabbits with the recently developed ms-DSEPI-T12 MRI in the present study. The usefulness of T_1 mapping with this technique to determine polymer distribution and clearance in the vitreous after intravitreal injection was demonstrated. Contrast agent MultiHance™ was quickly cleared from the eye in the first day post-injection. The non-biodegradable polymers PGH had slower clearance in vitreous compared with MultiHance. To examine the clearance of disulfide bond-containing biodegradable polymers and its degradation in the vitreous humor, intravitreal GDCP was investigated, and the results were compared with those of PGH and MultiHance. GDCP had faster clearance than PGH and had comparable clearance rate as MultiHance, suggesting that GDCP was broken into smaller fragments in the vitreous humor, possibly due to disulfide bond enzymatic degradation.

ACKNOWLEDGMENTS & DISCLOSURES

REFERENCES

1. Ghate D, Edelhauser HF. Ocular drug delivery. Expert Opin Drug Deliv. 2006;3(2):275–87.
2. Janoria KG *et al.* Novel approaches to retinal drug delivery. Expert Opin Drug Deliv. 2007;4(4):371–88.
3. Choonara YE *et al.* A review of implantable intravitreal drug delivery technologies for the treatment of posterior segment eye diseases. J Pharm Sci. 2010;99(5):2219–39.
4. Lee J *et al.* Temperature-sensitive biodegradable poly(ethylene glycol). J Biomater Sci Polym Ed. 2009;20(7–8):957–65.
5. Lee SS *et al.* Biodegradable implants for sustained drug release in the eye. Pharm Res. 2010;27(10):2043–53.
6. Meng F, Hennink WE, Zhong Z. Reduction-sensitive polymers and bioconjugates for biomedical applications. Biomaterials. 2009;30(12):2180–98.
7. Kim JO *et al.* Polymeric micelles with ionic cores containing biodegradable cross-links for delivery of chemotherapeutic agents. Biomacromolecules. 2010;11(4):919–26.
8. Mader K *et al.* Noninvasive *in vivo* monitoring of drug release and polymer erosion from biodegradable polymers by EPR spectroscopy and NMR imaging. J Pharm Sci. 1997;86(1):126–34.
9. Rudin M, Weissleder R. Molecular imaging in drug discovery and development. Nat Rev Drug Discov. 2003;2(2):123–31.
10. Li SK, Lizak MJ, Jeong EK. MRI in ocular drug delivery. NMR Biomed. 2008;21(9):941–56.
11. Richardson JC *et al.* Pharmaceutical applications of magnetic resonance imaging (MRI). Adv Drug Deliv Rev. 2005;57 (8):1191–209.
12. Rudin M *et al.* In vivo magnetic resonance methods in pharmaceutical research: current status and perspectives. NMR Biomed. 1999;12(2):69–97.
13. Wilson CG. *In-vivo* monitoring of dosage forms. J Pharm Pharmacol. 1998;50(4):383–6.
14. Kim H *et al.* Controlled drug release from an ocular implant: an evaluation using dynamic three-dimensional magnetic resonance imaging. Invest Ophthalmol Vis Sci. 2004;45(8):2722–31.
15. Kim H *et al.* Study of ocular transport of drugs released from an intravitreal implant using magnetic resonance imaging. Ann Biomed Eng. 2005;33(2):150–64.
16. Li SK, Jeong EK, Hastings MS. Magnetic resonance imaging study of current and ion delivery into the eye during transscleral and transcorneal iontophoresis. Invest Ophthalmol Vis Sci. 2004;45(4):1224–31.
17. Li SK, Molokhia SA, Jeong EK. Assessment of subconjunctival delivery with model ionic permeants and magnetic resonance imaging. Pharm Res. 2004;21(12):2175–84.
18. Kim SH *et al.* Assessment of subconjunctival and intrascleral drug delivery to the posterior segment using dynamic contrast-enhanced magnetic resonance imaging. Invest Ophthalmol Vis Sci. 2007;48(2):808–14.
19. Kim SH *et al.* Drug elimination kinetics following subconjunctival injection using dynamic contrast-enhanced magnetic resonance imaging. Pharm Res. 2008;25(3):512–20.
20. Molokhia SA *et al.* Examination of penetration routes and distribution of ionic permeants during and after transscleral iontophoresis with magnetic resonance imaging. Int J Pharm. 2007;335(1–2):46–53.
21. Molokhia SA *et al.* Examination of barriers and barrier alteration in transscleral iontophoresis. J Pharm Sci. 2008;97(2):831–44.
22. Molokhia SA *et al.* Transscleral iontophoretic and intravitreal delivery of a macromolecule: study of ocular distribution *in vivo* and postmortem with MRI. Exp Eye Res. 2009;88(3):418–25.
23. Liu X *et al.* Rapid simultaneous acquisition of T1 and T2 mapping images using multishot double spin-echo EPI and

automated variations of TR and TE (ms-DSEPI-T12). NMR Biomed. 2010;23(1):97–104.

24. Ke T *et al.* Biodegradable cystamine spacer facilitates the clearance of Gd(III) chelates in poly(glutamic acid) Gd-DO3A conjugates for contrast-enhanced MR imaging. Magn Reson Imaging. 2006;24(7):931–40.

25. Zong Y *et al.* Effect of size and charge on pharmacokinetics and *in vivo* MRI contrast enhancement of biodegradable polydisulfide Gd (III) complexes. J Control Release. 2006;112(3):350–6.

26. Schwartz B, Feller MR. Temperature gradients in the rabbit eye. Invest Ophthalmol. 1962;1:513–21.

27. Benjamin M, Synthesis, characterization, and determination of relaxivities for glycoamido-DTPA polymers for use as MRI contrast agents, Master Thesis, University of Cincinnati, 2006: Ch 2.

28. Bakri SJ *et al.* Pharmacokinetics of intravitreal ranibizumab (Lucentis). Ophthalmology. 2007;114(12):2179–82.

29. Gaudreault J *et al.* Pharmacokinetics and retinal distribution of ranibizumab, a humanized antibody fragment directed against VEGF-A, following intravitreal administration in rabbits. Retina. 2007;27(9):1260–6.

30. Kim H *et al.* The pharmacokinetics of rituximab following an intravitreal injection. Exp Eye Res. 2006;82(5):760–6.

31. Araie M, Maurice DM. The loss of fluorescein, fluorescein glucuronide and fluorescein isothiocyanate dextran from the vitreous by the anterior and retinal pathways. Exp Eye Res. 1991;52(1):27–39.

32. Maurice DM. Review: practical issues in intravitreal drug delivery. J Ocul Pharmacol Ther. 2001;17(4):393–401.

33. Urtti A. Challenges and obstacles of ocular pharmacokinetics and drug delivery. Adv Drug Deliv Rev. 2006;58(11):1131–5.

34. Mitra AK, Ophthalmic drug delivery systems. Second Edition, Informa Healthcare: New York, NY, 2003.